remote sensing

MDPI

Article

Land Cover Change and Fragmentation Within China's Ramsar Sites

Karen Kie Yan Chan [1], Zhehao Ren [1], Yufu Liu [1], Hang Song [1], Yuqi Bai [1,2] and Bing Xu [1,2,*]

[1] Ministry of Education Ecological Field Station for East Asian Migratory Birds, Department of Earth System Science, Institute for Global Change Studies, Tsinghua University, Beijing 100084, China; mail.kkychan@gmail.com (K.K.Y.C.); rzh18@tsinghua.org.cn (Z.R.); liuyufu18@mails.tsinghua.edu.cn (Y.L.); songh24@mails.tsinghua.edu.cn (H.S.); yuqibai@tsinghua.edu.cn (Y.B.)

[2] International Research Center of Big Data for Sustainable Development Goals, Beijing 100094, China

* Correspondence: bingxu@tsinghua.edu.cn

Abstract: The Ramsar Convention is a global endeavor for the protection of wetlands. However, there is limited research on its efficacy in safeguarding China's wetlands. This study aims to identify differences within Chinese Ramsar sites and their surrounding areas over the past three decades. This assessment was conducted using extensive land cover maps created by ESA CCI (European Space Agency Climate Change Initiative) through the classification of remote sensing data using the LCCS (Land Cover Classification System) and other systems specified by the IPCC (Intergovernmental Panel on Climate Change), in addition to ecoregion maps. Three primary assessments were performed: detection of change in land covers, fragmentation using effective mesh size and driver analysis using a random forest classifier. The findings indicate significant land cover changes within both Ramsar sites and their surrounding areas. Tree cover and grasslands showed the largest decrease in land cover while flooded shrubs and herbaceous cover showed the largest increase within the Ramsar sites. In contrast, urban areas had the largest overall change in the surrounding areas, with twice the increase compared to the areas within the Ramsar sites. Most land cover changes within the Ramsar sites occurred closest to their boundaries where more human interactions occurred. It was also found that the fragmentation of flooded vegetation and water was also greater in areas surrounding the Ramsar sites in comparison to areas within the sites. This study also identified human activity as the primary driver of all observed changes, especially for wetlands. The differences observed indicate the effectiveness of Chinese Ramsar sites in wetlands protection and provide invaluable information for future strategic planning.

Keywords: Chinese Ramsar site; change detection; land cover change; fragmentation; driver analysis

check for updates

Academic Editors: Michael Sprintsin and Deepak R. Mishra

Received: 25 December 2024
Revised: 28 January 2025
Accepted: 4 February 2025
Published: 4 March 2025

Citation: Chan, K.K.Y.; Ren, Z.; Liu, Y.; Song, H.; Bai, Y.; Xu, B. Land Cover Change and Fragmentation Within China's Ramsar Sites. *Remote Sens.* **2025**, *17*, 896. https://doi.org/10.3390/rs17050896

Copyright: © 2025 by the authors. Licensee MDPI, Basel, Switzerland. This article is an open access article distributed under the terms and conditions of the Creative Commons Attribution (CC BY) license (https://creativecommons.org/licenses/by/4.0/).

1. Introduction

Wetlands are fragile ecosystems that are integral to freshwater ecosystems and provide habitats to over 40% of the world's species with only 6.4% of the world's land surface [1–3]. The intricate relationships between hydrological and climatic conditions, local geography and biotic components within wetlands that sustain the high level of productivity and biodiversity are the very reason these ecosystems are especially vulnerable to changes that are occurring at ever increasing speed [4]. In response to the ever-increasing threats from the degradation and destruction of wetlands and as a response to the large-scale wetland destruction in Europe, the Ramsar Convention (The Convention on Wetlands of

International Importance, especially as Waterfowl Habitat) was created in 1971 [5]. It was the first of its kind and remains the only global convention for wetland protection, although additional international ecological agreements have also been created since.

Despite its significance, the Ramsar Convention is not without problems. As the Ramsar Convention is not considered to be a regulatory institution, it lacks the power to impose sanctions or punitive measures when regulations or agreements have been violated [6,7]. This lack of accountability and enforcement leaves the protection of Ramsar sites completely reliant on member countries with few incentives to honor their commitment, especially when faced with lucrative economic pressures with immediate payoffs such as urban development and rising land prices [8–10]. Furthermore, since member countries control the selection of Ramsar sites, selected sites are often already highly degraded or politically motivated rather than selected based on their ecological value [10]. Two examples of these sites are the Towra Point Nature Reserve in Australia and the Xuan Thuy Natural Wetland Reserve in Vietnam. While the Towra Point Nature Reserve is one of the most diverse estuarine wetlands, it has been highly degraded by heavy metals in sediment and water, which have impacted both the health and biodiversity of local and migrant species [11]. Additionally, the site is continuously exposed to numerous threats due to its close proximity to nearby chemical plants, a port and an international airport [11]. In comparison, the largest contiguous mangrove system in the Mekong delta was not selected as the only Ramsar site targeted towards the protection of mangroves in Vietnam. Despite the mangrove system in the Mekong delta being the more ecologically valuable option, the Xuan Thuy Natural Wetland Reserve was selected instead as a result of political and economic motivations [10].

Efforts aimed at protecting wetlands are further complicated as the ecological functions of protected areas are also dependent on habitats and resources located outside of their boundaries, where disturbances in the surrounding areas can substantially impact the ecological systems within the site and induce similar changes [12–14]. These changes result from alterations to the existing ecological flow, source–sink dynamics and exposures to human activity. This in turn causes the proliferation of light-, disturbance- or human-adapted species as a result of vegetation and wildlife disturbances caused by the reduction or elimination of habitats and fragmentation [13,15–17]. In conjunction with the issues inherent to Ramsar sites, there are few assessments of the effectiveness of Ramsar sites in the protection of wetlands in terms of both land cover changes and the degree of fragmentation within wetlands [10,13,18]. The limited research on landscape metrics, wetlands and Ramsar sites is a further reflection of this. An article search conducted with the key words "landscape metrics", "wetlands", and "Ramsar'" on 2nd January 2024 identified only 25 relevant articles within the top 80 results. However, this area of study has been gaining traction as the large majority of these were published after 2016, with over 30% of these articles published in the last three years. The largest clusters were focused on a single site over 26 to 35 years with three to nine revisits.

The aim of this study is to compare the land cover changes within Ramsar sites in China and the immediate surrounding areas over the past three decades as it is one of the largest countries in Asia where the largest total wetland loss has occurred. In order to consider the effect of abiotic components, the study sites are further delineated based on eco-provinces and eco-biomes. Next, landscape metrics, such the mean effective mesh size, were applied to explore the effects of land cover changes on fragmentation in the study area. Finally, a change analysis was applied to both overall land cover changes and to a subset solely based on wetlands changes.

2. Materials and Methods

2.1. Study Sites

Asia has the largest wetland loss by area with a total loss of 2.65 million km^2 as of 2009 [18]. China is one of the largest countries in Asia, and as of 2020, it has a land surface area of 9,424,702.9 km^2 with 3.8% of it comprising various types of wetlands that provide 54.9% of the country's total ecosystem services [19–21]. China has already lost nearly 29% of its wetlands [18,20,21]. There are currently 82 designated Ramsar sites covering 76,479.0 km^2. Of these 82 sites, 43 sites had available site boundaries as of September 2019 [22,23]. These sites are distributed across 19 of the 34 provinces, municipalities, autonomous and administrative regions and are located within 8 of China's 17 Udvardy eco-provinces (Figure 1, Table S1). Of these sites, the four that are shaded on S1 are distributed over multiple eco-provinces.

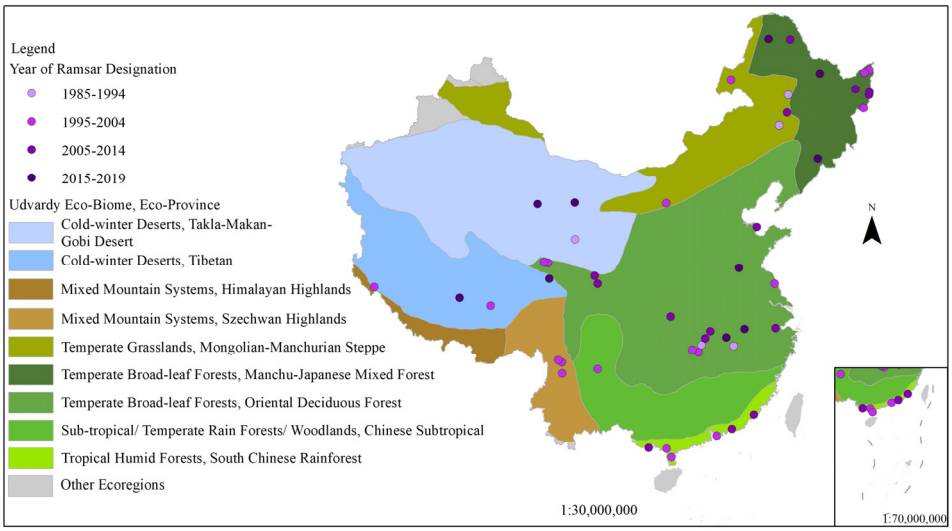

Figure 1. Ramsar Sites and Udvardy ecoregions in China.

The WGS 1984 was used as the Geographic Coordinate System for the maps and datasets within this study with world cylindrical equal area projection utilized where applicable. An overview of the methodology may be found in the Methodology Flowchart (Figure 2). The Ramsar vector dataset was used to create both the internal and external buffers shown in Section 1B and to extract the study sites from the Integrated LC and IPCC Classification Database in Section 1C to facilitate further change analysis in Section 2 (Figure 2). Concurrently, the ESA CCI datasets based on the 22 LCCS classes and the 9 IPCC classes were used to generate the Integrated LC and IPCC Classification Dataset shown in Section 1C. The resultant extracted integrated LC and IPCC classification database described in Section 2 was then integrated with Ecoregion Maps to analyze changes within the various ecoregions across the three decades. The initial integrated annual dataset created in 1C was also used in Section 3 for landscape analysis (Figure 2). The resultant wetland changes in the internal areas of the site were further extracted to check for change drivers in Section 4 (Figure 2).

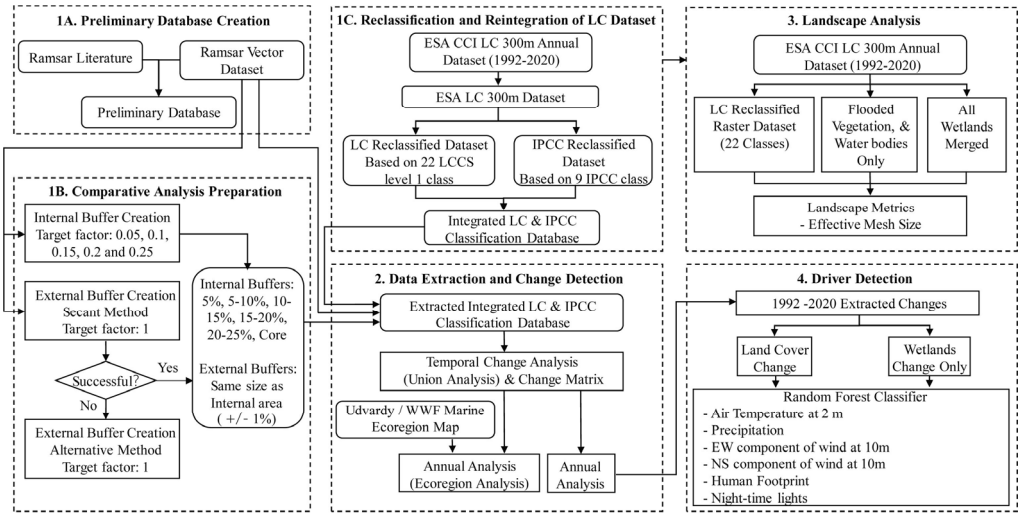

Figure 2. Methodology Flowchart.

2.2. Ramsar Vector Datasets

Vector files for the Ramsar site boundaries were compiled from two sources. Ideally, vector files on the boundaries of all Ramsar sites in China would be available from the Ramsar Sites Information Service [23]. However, there were sites where the site boundaries were not available. For the sites without available boundaries, files containing the centroids of the remaining sites with attributes containing site names, and descriptions were exported so they could be matched to sites in the World Database on Protected Areas (WDPA) [22]. These centroids were first matched to sites in the WDPA_poly_Sept2019 database by name if their "DESIG" or "DESIG_ENG" attribute contained the key word "RAMSAR". If no further match was found, the centroids of the remaining Ramsar sites were overlayed on top of all of the available site boundaries in the WDPA_poly_Sept2019 database without the key word "RAMSAR". These WDPA sites were then used if (1) the site name on the WDPA database matched with the those provided by Ramsar, or (2) a Ramsar centroid was located within the site boundary of a WDPA site. In rare cases, a Ramsar centroid was found to be located within multiple WDPA sites. Where this occurred, the vectors of all WDPA site boundaries were combined to create the largest possible protected area boundary to act as a proxy for the Ramsar site boundary.

2.3. Internal and External Buffers

The creation of the internal and external buffers is summarized in Section 1B of Figure 2. Two sets of buffers were created in order to analyze changes in the surrounding areas and the impact of fragmentation within the study sites. The exterior buffer of each Ramsar site is equal in area to the site itself to an accuracy of 1% and is used to account for the impact of changes to the surrounding area. To achieve this, a series of calculations based on the QGIS Buffer by Percentage Plugin were performed using Python 2.7 to calculate the buffer lengths [24]. The initial buffer length was calculated as:

$$IBL = 0.1 \times (BW + BH) \quad (1)$$

where IBL, BW and BH represent the initial buffer length, the calculated width and the height of bounding box. A second calculation for the error was calculated using

$$CE = \frac{SA}{IA} - TF \quad (2)$$

where CE represents the calculated error, the SA represents the surrounding area (area of the buffer) generated from the calculated buffer length and IA represented the initial area (area of the original Ramsar site), while TF represents the target factor, where the desired target size is a multiple of the initial area which is set to 1 to achieve a scaled area that is identical to the size of the Ramsar sites. This error calculation ensures that the SA, when compared to the IA, is identical to the TF desired. Finally, an iterative secant method was used to calculate the appropriate buffer length:

$$BL = secant[CE,\ BI, 2 \times BI,\ geometry,\ segments,\ IA,\ TF] \tag{3}$$

where BL is the appropriate buffer length, and BI as the initial guess for the buffer. In addition, *geometry* represents the initial geometry of the polygon while *segments* contained details of the polygon's line segments. For cases where this method failed to calculate the appropriate buffer lengths, an alternative method was used and generated using ArcGIS 10.3. First, the lengths of the bounding envelope were calculated using:

$$X_{length} = X_{max} - X_{min} \tag{4}$$

$$Y_{length} = Y_{max} - Y_{min} \tag{5}$$

These were then used to calculate the area of the bounding envelope:

$$EA = X_{length} \times Y_{length} \tag{6}$$

where EA represents the enveloped area. To adjust for the differences between the Ramsar site polygon's area and the bounding box, a polygon adjustment factor (PAD) was calculated using

$$PAD = \frac{PA}{EA} \tag{7}$$

where PA is the area of the Ramsar Polygon. The use of this adjustment ensures the resultant buffer will reflect the actual area of the Ramsar site.

Using Equations (4) and (5), the hypotenuse of the bounding box was found. This diagonal distance was calculated as

$$EH = \sqrt{X_{length}^2 + Y_{length}^2} \tag{8}$$

where EH is the envelope hypotenuse. The hypotenuse and the polygon adjustment factor were then used to calculate the initial buffer length using:

$$IBL = \frac{EH}{3} \times \frac{1}{2} \times PAD \tag{9}$$

where IBL is the initial buffer length. Each time the area of a square is doubled, the hypotenuse is increased by 0.41 times. Therefore, a value of $\frac{1}{3}$ was chosen to approximate the increase in hypotenuse required to double the area. This increase in the hypotenuse length is equivalent to the initial buffer length. The additional division by 2 gives the value required for ArcGIS to apply the increase equally in all directions. Once the buffer has been created, the error between the scaled area and the initial area can be computed to ensure the correct buffer size has been achieved. The error is calculated as:

$$CE = \frac{SA}{IA} \tag{10}$$

If the calculated error (*CE*) was greater than 0.01, further iterations were performed to adjust the buffer length (*BL*), starting with the following equation:

$$BL_1 = BL_0 \times CE_0 \quad (11)$$

where BL_0 is the initial buffer length, and CE_0 is the calculated error of the initial buffer length as defined by the following:

$$BL_0 = IBL \quad (12)$$

$$CE_0 = CE_{IBL} \quad (13)$$

After the initial calculation, the subsequent iterations follow the formula:

$$BL_n = BL_{n-1} \times CE_{n-1} \quad (14)$$

to calculate a new buffer length. If the *CE* remains greater than 0.01, repeated calculations using Equation (15) are carried out to reduce the *CE* so that becomes less than 0.01.

The second set of buffers generated are the internal buffers and they are created using a simplified version of the alternative method described in Equation (9) with the following equation:

$$IBL_{interior} = X_{length} \times PAD \times TF \quad (15)$$

where X_{length} is the length of the bounding box surrounding the Ramsar site. These are generated using ArcGIS 10.3 with a code written in python 2.7 for batch processing. The target factors (*TFs*) used to calculate the internal buffers were 0.05, 0.10, 0.15, 0.20 and 0.25 and represent the varying distances (in terms of percents) away from the Ramsar site boundary. In order to analyze changes that occurred within the sites at distances of less than 5%, 5–10%, 10–15%, 15–20% and 20–25% from the site boundary, all buffers were created by subtracting the area of the previous buffer, with the exception of the initial buffer, which corresponded to a TF of 0.05. This ensured that there were no overlaps in the area of each internal buffer. The remaining area of the Ramsar sites represents the area more than 25% away from the site boundary and was also created through the subtraction of the buffer created using the *TF* of 0.25 from the initial Ramsar site. Once these buffers were created, they were transformed using the exact projection and grid size of the land cover dataset so that an exact grid match could be extracted.

2.4. Ecoregion Maps

Ecoregion maps are delineated based on species composition, geomorphology, soil types, and local climates. As such, they compress a wealth of information into a manageable data source. The integration of these ecoregion maps provides greater insights into the changes observed than a study based solely on land cover observations [18,25,26]. For this study, the vector files of the terrestrial ecoregion map created by Udvardy and the map of the WWF Marine Ecoregions of the World were downloaded from the FAO and WWF site, respectively, on 9th October 2019 [27,28]. These maps were then integrated with the Ramsar site boundaries and their surrounding areas.

2.5. Land Cover Dataset

This study used the European Space Agency Climate Change Initiative's (ESA CCI) CCI-LC maps at a resolution of 300 m from 1992 to 2020 to evaluate land cover changes that occurred within the Ramsar site boundaries and in the adjacent areas [29]. Annual land cover maps were created using five satellite systems and the UN Land Cover Classification

System (LCCS) developed by the FAO with an accuracy between 71.5% and 75.4% [30]. The LCCS classification system contains a global legend with regional subdivisions whenever possible (Table S2) and is also compatible with the GLC2000 and GlobCover 2005 and 2009 products. In order to maintain a consistent classification throughout the study, only the global legends were used (Table S2) as regional subdivisions were not always available. An additional conversion table was also provided to convert the LCCS classification into the nine classes used by the Intergovernmental Panel on Climate Change (IPCC) (Table S2) [30]. There is also one further limitation inherent to the dataset: once a change has occurred, it must still be observable the following year in order for the change to be considered valid. Otherwise, the change will not be registered. Compared to similar datasets with higher spatial resolutions at 30 m such as the China Land Cover Dataset (CLCD) and GLC_FCS30D, the CCI-LC 300 m has more defined classes within wetlands than CLCD and a greater temporal data availability within the 1992 to 2000 period than GLC_FCS30D [30–32].

2.6. Change Detection

Since the CCI-LC 300 m maps require land cover changes to be observed within both the LCCS classes and the IPCC classes in order to be considered valid, the land cover data were reclassified into two datasets based on the 22 LCCS classes with accuracy assessments and their corresponding IPCC classes to become the Integrated LC and IPCC Classification Dataset in Section 2 of Figure 2 [30]. Once the study sites had been extracted, a union analysis was then applied to the Extracted Integrated LC and IPCC Classification Dataset. Within the Extracted Integrated LC and IPCC Classification Dataset, land cover maps for consecutive years were grouped into consecutive pairs. These consecutive pairs were then analyzed where the earlier map was designated as the "initial" and the latter map "final". This was performed using ArcGIS 10.3 with a code written in python 2.7 for batch processing until all consecutive pairs from 1992 to 2020 were analyzed. Individual land cover changes were also analyzed using two land cover change matrices created from the land cover descriptions provided by ESA. These matrices focus on the respective changes towards the "final" land covers as well as those away from the "initial" land covers. This not only provided insights into the specific changes that occurred but also insights into the annual overall change that occurred. In addition to the change analysis performed on each individual land cover class, additional ones were performed on an aggregate of all flooded vegetation, and on an aggregate of all wetland types which included water bodies. The cumulative change is also referred to as the total change within this study and was calculated as the sum of the magnitude of all changes experienced throughout the study period regardless of if the change experienced was a loss or a gain. In comparison, the overall change is the sum total of changes with respect to their directionality. This study focuses on the analysis of the land cover changes experienced within China's Ramsar sites as a whole, their surrounding areas, the regional and provincial differences within Ramsar sites, the internal distribution of these changes and an individual site selected as a case study.

2.7. Landscape Analysis

The effective mesh size (m_{eff}) quantifies the probability that two randomly selected points in the landscape are located within the same patch [33]. This metric was as a measure of the level of fragmentation since a decrease in the m_{eff} indicates an increase in fragmentation [10,33]. Although the m_{eff} for each class was calculated with the package Pylandstat using Python 3.6 created by Bosch in 2019 [34], it can also be calculated using the following:

$$m_{eff} = \frac{1}{A_{total}} \sum_{i=1}^{np} A_i^2 \quad (16)$$

where np is the total number of patches, A_{total} represents the total area and A_i represents the area of patch i. Not only was the m_{eff} calculated for each class, it was also calculated for wetlands (flooded vegetation and waterbodies) as a whole. When multiple sites are considered as a whole, the fragmentation of the whole area is delineated using the mean effective mesh size (M_{eff}) and calculated using the mean m_{eff} of all sites. For this study, the overall changes in fragmentations within the Chinese Ramsar sites as a whole and their external areas were studied, in addition to a case study of a selected site.

2.8. Driver Analysis

Due to the limitations of the available data on change drivers, driver analysis was only performed on the changes between 2000 and 2020. In order to perform the driver analysis, the latitude and longitude coordinates of the centroids of each pixel where changes were observed were calculated. The initial and final land cover classes, in addition to the land cover change experienced, were then integrated with the latitude/longitude coordinates. Anthropogenic drivers such as human footprint and night-time lights, as well as natural drivers such as air temperature at 2 m (min, mean, max), precipitation (min, max, sum), the E-W component of wind at 2 m (mean, max) the and N-S components of wind at 10 m (mean) that were available from the ERA5 reanalysis dataset were selected as possible drivers [35–37]. The random forest model was chosen to perform the driver analysis due to its ability to handle complex datasets and model non-linear relationships [38]. This classifier was used to construct multiple decision trees and rank the drivers based on their contributions to change, and was used to identify the most significant drivers [38]. The importance of each driver was then assessed based on the average reduction in impurity (Gini impurity) across all trees. To ensure the predictability of the results, the number of estimators in the random forest classifier was configured to 100 with the random state set to 42, while the remaining parameters were left at the default settings. The equations used to construct the decision trees, their predictions, and the importance of each driver were calculated using Equations (S1)–(S4) in Python 3.11.4. This process resulted in an annual feature importance value for each driving factor that equals to an annual sum of 1 when the feature importance values of all driving factors are summed together. For this study, two sets of driver analysis were performed, one set for all changes observed and another set for the wetland changes observed both within the Ramsar sites and their surrounding areas. These resulted in a four sets of feature importance values for each of the change drivers for each year from 2001 to 2020.

Despite uncertainty in the ESA CCI land cover dataset as well as other data used in this study, the random forest (RF) model provides several advantages. First of all, this model is inherently robust against noise and measurement errors due to its ensemble nature, where each decision tree is trained on a random subset of the data, and predictions are averaged across the trees. This reduces the impact of outliers or noisy samples in the training data. Second, the RF model leverages feature importance metrics, allowing us to identify and minimize the influence of less reliable features on the final predictions. Moreover, we ensure that the quantity of data for training samples is sufficient by removing changes with too few (less than 10) samples to minimize model error and to ensure a good general performance. Additionally, a series of two tailed T-tests comparing each of the possible drivers was carried out to test if that the identified importance was statically significant.

3. Results

Cumulatively, a total of 4000.2 km^2 or 6.6% of the total area within Chinese Ramsar sites experienced changes between 1992 and 2020 (Table S3). In comparison, the total changes included in the surrounding areas totaled 3532.3 km^2 or 5.6% of the total area

(Table S3). The majority of the changes observed were either a complete alteration of a singular land cover class or a mosaic land cover which was completely replaced by a single type of land cover. These changes represent over 84% of the land cover changes observed within the Ramsar sites and over 80% of the changes in the surrounding areas (Table S3). The remaining changes consist of alterations within mosaic land covers where changes were observed but the exact contributions to the land cover are uncertain.

3.1. Land Cover Changes and the Contributors of Wetland Changes

Within Ramsar sites, the three land cover classes that experienced the largest cumulative changes were grasslands (LCCS 130), water bodies (LCCS 210) and a mosaic of tree, shrub and herbaceous cover (LCCS 150). The cumulative changes experienced by these land cover classes totaled 4115.7 km^2, 1873.4 km^2 and 701.6 km^2, respectively (Table S3). Comparatively, the largest overall changes experienced were a loss of 347.4 km^2 for tree cover (LCCS 70), and 293.3 km^2 for grasslands (LCCS 130) with a gain of 318.1 km^2 in flooded shrub or herbaceous cover (LCCS 180). When comparing overall changes with the cumulative changes observed in Ramsar sites, the overall changes observed are smaller in magnitude than the cumulative changes as this takes into account losses as well as increases.

Meanwhile, in the surrounding areas, grasslands and a mosaic of tree, shrub and herbaceous cover were also land cover classes that experienced the largest cumulative changes with the addition of a mosaic of cropland, tree, shrub and herbaceous cover (LCCS 40). The cumulative changes experienced by these land cover classes totaled 2028.2 km^2, 852.6 km^2 and 706.7 km^2. Like their counterparts within the Ramsar sites, the overall changes observed were much lower than their cumulative change ranging between 9.8 km^2 and 220.5 km^2 (Table S3). However, the largest overall land cover change in the surrounding areas with comparable values to those within the Ramsar sites were in urban areas, with an increase of 343.1 km^2 (LCCS 190), and mosaic cropland, tree, shrub and herbaceous cover (LCCS 40), with a loss of 220.5 km^2.

Within the wetland classes in Ramsar sites, the majority of the cumulative changes was observed within water. However, the majority of the overall changes were concentrated in flooded shrub and herbaceous cover within Ramsar sites (Table S3). The loss of wetlands comprised various wetland classes within Ramsar sites and mainly resulted in its conversion into grasslands (28.3%), other wetlands classes (27.7%), croplands (15.9%) and bare areas (12.2%) (Table 1). In comparison, the largest gains of wetlands within Ramsar sites were from grasslands (45.4%), other wetlands (20.7%), tree cover (17.9%) and bare areas (6.1%) (Table 1). Within individual wetland classes, the largest gains of water were conversions from grasslands (63.6%) and tree cover (11.4%), while the largest losses of water were conversions into grasslands (30.0%), other wetlands (26.4%) and croplands (16.7%). Comparatively, the largest gains of flooded shrub or herbaceous cover were conversions from other wetlands (64.3%) and tree cover (34.9%), and the largest losses were conversions into other wetlands (57.4%) and urban areas (32.8%) (Table 1).

For wetlands within the surrounding areas, the majority of the cumulative changes, as well as overall changes, were observed within water (Table S3). Similarly, the largest changes in the surrounding area were also similar to those observed within the Ramsar sites. The majority of the loss of wetlands comprising various wetland classes were converted into other wetlands (39.1%), grasslands (14.7%) and croplands (14.5%). The largest gains were also converted from other wetlands (25.3%), grasslands (20.6%) and tree cover (17.8%). There were also similar observations between the various wetlands and their Ramsar counterparts, with an increase in conversions between wetlands, and a lower percentage of wetland conversion from other land covers. However, it should also be noted that the

conversion of wetlands to urban areas was three times the amount observed within the Ramsar sites at 6.6%.

Table 1. Contributors to wetland changes within Chinese Ramsar sites and their surrounding areas (ext).

Land Cover(s) Present	LCCS Land Cover Classes	All Wetlands				Water				Shrubs or Herbaceous Cover (Flooded)			
		Gains (%)		Losses (%)		Gains (%)		Losses (%)		Gains (%)		Losses (%)	
		Ramsar	Ext	Ramsar	Ext	Ramsar	Ext	Ramsar	Ext	Ramsar	Ext	Ramsar	Ext
Bare Area	200	6.1	9.6	12.2	7.4	8.5	13.2	12.9	9.0				
Cropland	10, 20	2.9	10.8	15.9	14.5	3.5	10.2	16.7	17.6	0.6	12.0	3.0	0.6
Cropland, Trees, Shrubs, Herbaceous cover	30, 40	5.3	12.8	4.6	6.3	7.3	17.3	4.8	7.6				
Grassland	130	45.4	20.6	28.3	14.7	63.6	27.8	30.0	18.0		1.0		
Shrubland	120	0.4	0.9	0.2		0.5	1.3	0.2			0.1		
Tree cover	50–90	17.9	17.8	0.7	1.4	11.4	16.9	0.4	1.1	34.9	22.0	5.0	2.6
Tree, Shrub, Herbaceous cover	100, 110, 150	1.4	2.2	7.7	8.0	1.8	2.9	8.1	9.6	0.1	0.2	0.2	0.7
Urban Area	190			2.2	6.6			0.4	1.9			32.8	28.2
Permanent Snow and Ice	220												
Wetlands:													
Water	210	18.3	17.7	3.2	12.3					64.3	64.6	57.4	67.5
Shrub or Herbaceous cover (Flooded)	180	2.4	7.6	24.5	26.8	3.3	10.4	26.0	32.7				
Tree cover (Fresh/Brackish)	160										0.1		
Tree cover (Saline)	170			0.5	2.1			0.4	2.5			1.7	0.4

3.2. Regional and Provincial Distribution of Land Cover Change

Even as the contributions of wetland changes differ between the various wetland classes, regional and local differences also affect the distribution of land cover changes within the nine ecoregions in China with Ramsar sites. The majority of the changes within land cover types are concentrated within the four eco-provinces of the Oriental Deciduous Forest, the Tibetan Cold-winter deserts, the Mongolian–Manchurian Steppe and the Manchu–Japanese Mixed Forest. The Oriental Deciduous Forest had the highest overall changes with increases in flooded vegetation (192.5 km^2) and urban areas (122.6 km^2), and a decrease in shrubland (5.2 km^2) (Table S4). Comparatively, the Tibetan Cold-winter deserts had the highest overall increase for water (444.0 km^2) and an overall decrease in grasslands (350.4 km^2). The Mongolian–Manchurian Steppe ecoregions had the largest overall increases in cropland (164.0 km^2) and bare areas (44.8 km^2) (Table S4) and the largest overall decreases in tree cover (297.0 km^2) and mosaics of tree, shrub and herbaceous cover (19.5 km^2) were in the Manchu–Japanese Mixed Forest.

It should be noted that the majority of the total changes in mosaics of tree, shrub and herbaceous cover as well as urban areas, tree cover and flooded vegetation were highly concentrated in a single ecoregion, albeit different ecoregions for the various land covers. For a mosaic of tree, shrub and herbaceous cover, over 95% of the total changes were observed and concentrated in the Manchu–Japanese Mixed Forest ecoregion. This region also experienced close to 77% of the total changes in tree cover (Table S4). In contrast, the total changes within the urban area and flooded vegetation were also concentrated in the Oriental Deciduous Forest where over 85% of the changes in urban area and over 64% of the changes in flooded vegetation were located (Table S4).

The majority of the land cover changes were also concentrated in seven of the eighteen administrative regions with provincial status in China with Ramsar sites. The largest overall

increases in croplands (116.2 km^2) as well as the largest overall loss of tree cover (283.2 km^2) and mosaics of tree, shrub and herbaceous cover (19.5 km^2) were observed in Heilongjiang (Table S5). In the same manner, Tibet had the largest gains in water (444.0 km^2), along with the largest loss of grasslands (339.5 km^2), while Hubei had the largest gains in urban areas and flooded vegetation with overall increases of 68.8 km^2 and 143.4 km^2, respectively. Lastly, Inner Mongolia had the largest overall increase in bare areas at 51.3 km^2 (Table S5).

Unlike the distribution of land cover changes within ecoregions, which are often highly concentrated, land cover changes are more dispersed with a few exceptions. The concentration of changes in mosaics of tree, shrub and herbaceous cover was highly concentrated within Heilongjiang with over 95% of the changes observed (Table S5). In addition, Heilongjiang also had a high concentration of changes in tree cover with close to 75% of the changes observed. Other provinces with a high concentration of total land cover changes include Hubei for urban areas (47.8%) and flooded vegetation (42.6%) and Tibet for grasslands (46.8%) (Table S5). The remaining land covers were far more dispersed among the various provinces. Even when there was a higher concentration of changes within a single province, the changes constituted less than 40% of all the changes observed for that particular land cover.

3.3. Internal Distribution of Land Cover Changes

Further examination of the internal distribution of land cover changes showed that many of the largest changes occurred closest to the site boundaries for the majority of the land cover changes with few exceptions. Over 50% to 76.5% of the provinces with changes in flooded vegetation, bare areas, urban areas and croplands had the highest concentration of changes within the 5% buffer closest to the site boundaries (Table S6). These percentages increased from over 60% to over 90.9% of the provinces when both the outermost buffers (5% and 10% buffer) were examined together. For provinces where changes to croplands were experienced, the changes were observed within the 5% or 10% buffers for 90.0% of the provinces (Table S6). This was also observed for changes in bare areas (88.8% of the provinces with changes). These percentages decreased for flooded vegetation (64.7% of provinces with changes) and urban areas (61.5%). In contrast, the remaining land covers continued to have provinces where the greatest change was located within the 5% and 10% buffer but to a much smaller degree (Table S6). These land covers include tree cover (47% of provinces with changes), a mosaic of tree, shrub and herbaceous cover (42.9%) and water (26.7%).

However, twelve provinces experienced changes where a large majority (70%) of the changes for at least one land cover occurred within the 5% buffer area of the Ramsar sites (Table S6). Within these provinces, there were seven provinces where changes to urban areas represented over 70% of the total change located within the 5% buffer area. Additionally, bare areas and a mosaic of tree, shrub, herbaceous cover dominated in three provinces where over 75% of the changes were located within the 5% buffered area. Furthermore, Liaoning, Zhejiang, Yunnan, Shanghai and Guangxi had multiple types of land covers for which the large majority of the changes were located within the outermost buffer (Table S6). These provinces also experienced changes which were entirely located within the 5% buffer. These were observed for a mosaic of tree, shrub and herbaceous cover within Liaoling and Hubei, bare areas within Jiangsu and Shandong, flooded vegetation for Yunnan and urban areas within Hong Kong and Shanghai (Table S6). It is important to note that Hong Kong and Shanghai are the only two cities with provincial administrative status containing Ramsar sites.

In contrast, five provinces had land cover changes that generally occurred beyond the 5% buffer area. Unlike those occurring within the 5% buffers, all but one occurred in

different provinces. Jiangsu experienced all of its changes in tree cover in the 10% buffer as did Shanghai for its changes in bare areas (Table S6). Heilongjiang experienced the majority of its changes in water (76.8%) in the 25% buffer as did Guangdong for its changes in mosaics of tree, shrub and herbaceous cover (74.3%). Inner Mongolia was the only province in which the majority of changes occurred outside the 5% buffer for two types of land cover. Changes in mosaics of tree, shrubs and herbaceous cover also occurred entirely within the 25% buffer and 90% of changes in urban areas occurred in the same buffer area (Table S6).

3.4. Fragmentations Within Ramsar Sites and Its Surrounding Areas

Fragmentation is commonly evaluated using the effective mesh size (m_{eff}) or the mean effective mesh size (M_{eff}), and larger values are indicative of a more cohesive landscape with larger patch sizes and less fragmentation. Water was the least fragmented of the three landscapes within the Ramsar sites in 1992 with an M_{eff} of 178.6 km^2, followed by flooded vegetation at 26.2 km^2 and urban areas, being the most fragmented at 0.03 km^2 (Figure 3).

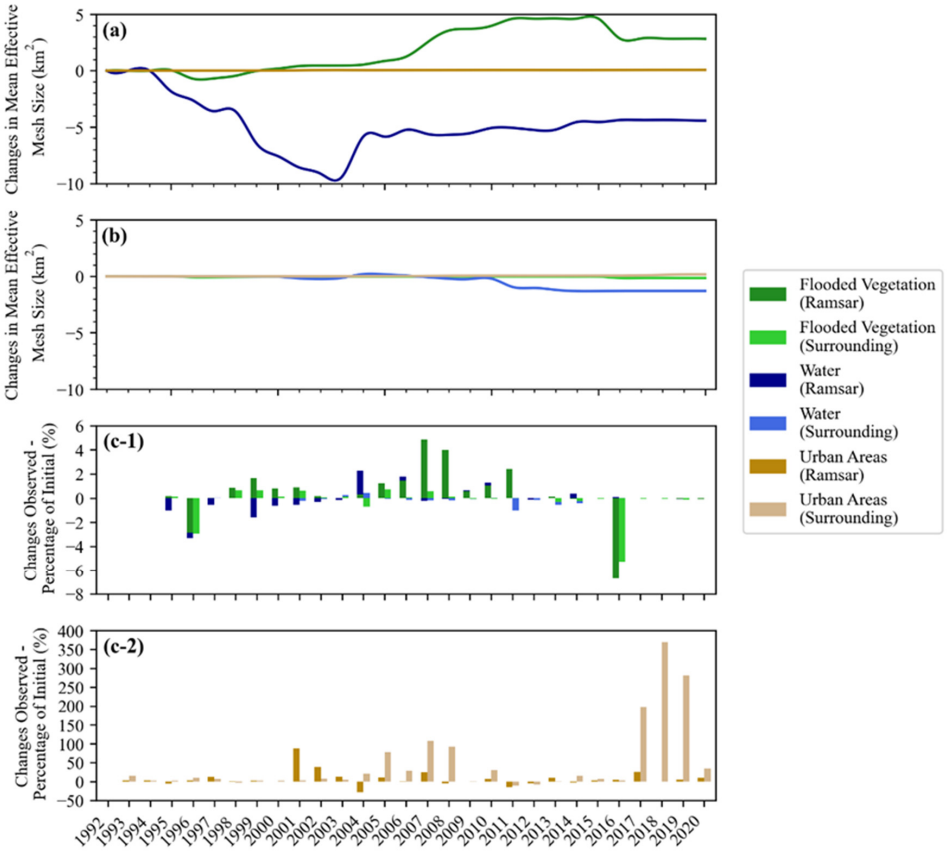

Figure 3. Changes in China's mean effective mesh size of flooded vegetation, water and urban areas. Figure (**a**) shows the change in mean effective mesh size for Ramsar sites within China. Figure (**b**) shows the change in mean effective mesh size for the surrounding areas within China. Figure (**c-1**) shows the change in mean effective mesh size as a percentage of the initial value in both the Ramsar sites and surrounding areas for the various land covers. Figure (**c-2**) shows the change in mean effective mesh size as a percentage of the initial value in both Ramsar sites and its surrounding areas for the various land covers where the percentage change is above 10%.

When these initial values were compared to their counterparts in the surrounding areas, both flooded vegetation and water experienced greater fragmentation, while urban areas had less fragmentation. The largest differences between the initial fragmentation observed within the Ramsar sites and their surrounding areas were for flooded vegetation, which was far more fragmented in the surrounding areas with an initial M_{eff} that was less

than a tenth of those observed within the Ramsar sites. Comparatively, the initial M_{eff} of water and urban areas in the surrounding areas were close to a third of their counterparts within Ramsar sites with initial values of 72.4 km^2 and 0.01 km^2, respectively (Table S7).

Over the span of three decades, the M_{eff} within the Ramsar sites increased for both flooded vegetation (M_{eff} of 2.8 km^2 by 10.7%) and urban areas (0.06 km^2 by 200.0%), which indicates an overall decrease in fragmentation (Figure 3, Table S7). However, water experienced an overall decrease in its M_{eff} of 4.4 km^2 (by 2.5%), which resulted in an increase in fragmentation. Similarly, urban areas in the surrounding areas of Ramsar sites also experienced an increase in the M_{eff} of 0.17 km^2 (1700.0%), with a concurrent decrease in M_{eff} for water of 1.3 km^2 (1.8%) (Figure 3, Table S7). In contrast, there was a decrease in the M_{eff} of flooded vegetation of 0.2 km^2 (6%). These results indicate that the surrounding areas experienced an increase in fragmentation for both flooded vegetation and water, and a decrease in fragmentation for urban areas.

A comparison of M_{eff} values between Ramsar sites and their surrounding areas also reveals useful information regarding evaluating its effectiveness in slowing or preventing fragmentation. These comparisons are all unique for the three different landcovers. The M_{eff} values show that the Ramsar sites and its surrounding areas both saw an increase in the fragmentation of water, but a comparison of their M_{eff} values (174.2 km^2 within Ramsar sites and 71.1 km^2 for its surrounding areas) reveal that the fragmentation within the Ramsar sites was greater (Figure 3, Table S7). These observations are in contrast to the changes observed within urban areas where the decrease in fragmentation was greater in the surrounding areas with a final M_{eff} of 0.18 km^2 compared to the final M_{eff} of 0.09 km^2 within the Ramsar sites. Over the same period, the Ramsar sites experienced a decrease in the fragmentation of flooded vegetation while the surrounding areas experienced an increase in fragmentation.

Further comparison of total land cover along with changes in the mean effective mesh size within Ramsar sites gives greater context to the fragmentation observed over the past three decades. Urban areas within Ramsar sites experienced an increase in total area of 149.7 km^2 (270.8%) along with an increase in M_{eff} of 0.06 km^2 (208%) (Figures 3 and 4, Tables S7 and S8). The greater total area along with larger M_{eff} values signifies an increase in the mean effective patch sizes for urban areas, indicating the growth of larger overall patches. The same trend where an increase in total land cover area resulted in a decrease in fragmentation was also observed in flooded vegetation and water bodies within the Ramsar sites (Figures 3 and 4, Tables S7 and S8). It is important to note that there was a sharp decrease in the water land cover areas from 1992 to 2002 and although this increased after 2002, the total area has remained less than the area in 1992.

A comparison of the changes between the total land cover and the mean effective mesh size was also compared for the surrounding areas. In these areas, urban areas had the largest overall increase in surface area (339.4 km^2 or 433.0%) with a significant increase in M_{eff} (0.17 km^2 or 1700.0%) indicating a significant decrease in fragmentation (Figures 3 and 4, Tables S7 and S8). However, the other land cover types experienced increases in their total area in conjunction with a decrease in M_{eff}. The respective increase in area and decrease in M_{eff} for flooded vegetation were 69.9 km^2 (41%) and 0.2 km^2 (6.0%), while those for water were 96.8 km^2 (1.5%) and 1.3 km^2 (1.8%) (Figures 3 and 4, Tables S7 and S8). These observations indicate that despite the increases in flooded vegetation and water within the surrounding areas, the overall patch size continued to decrease as the number of patches increased, resulting in greater fragmentation. Furthermore, the M_{eff} for flooded vegetation and water in 2020 continues to be significantly higher than those in the surrounding area, indicative of overall lower fragmentation (Table S7).

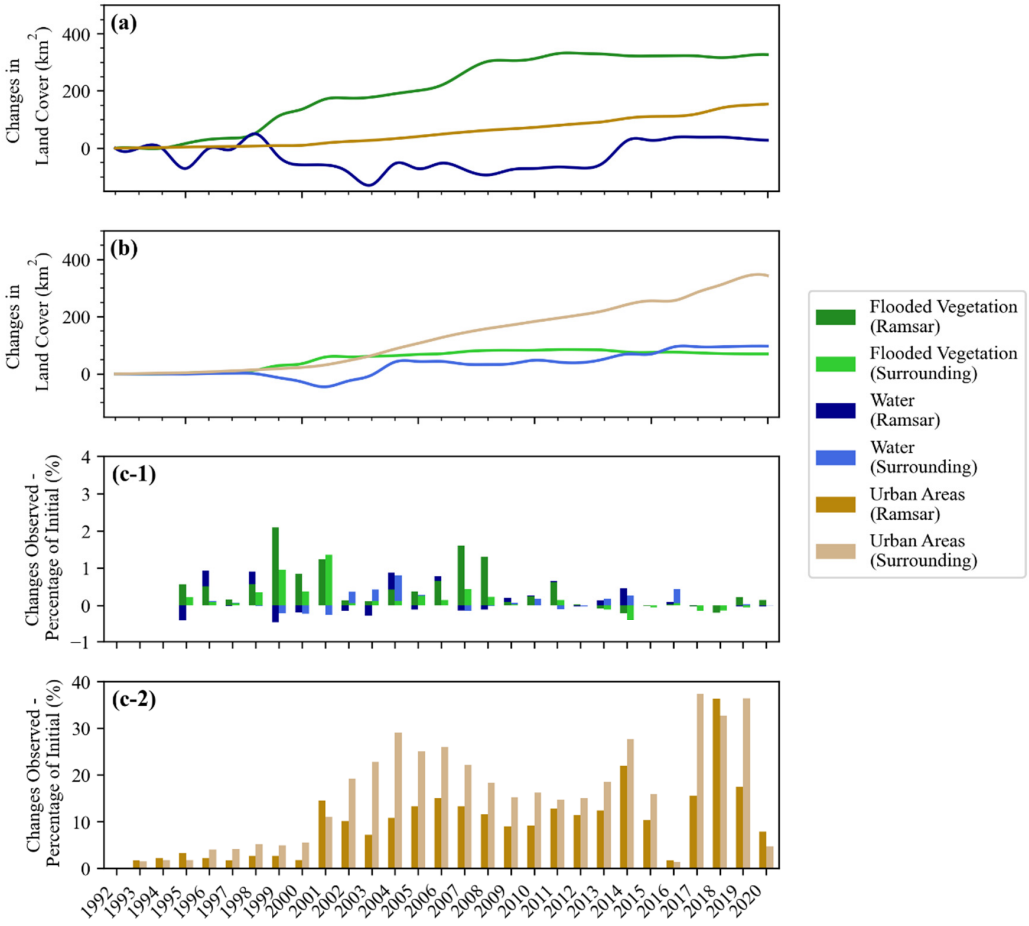

Figure 4. Changes in China's total area of flooded vegetation, water and urban areas. Figure (**a**) shows the change in total area for Ramsar sites within the land covers. Figure (**b**) shows the change in total area for surrounding areas within the land covers. Figure (**c-1**) shows the change in total area as a percentage of the initial value in both Ramsar sites and its surrounding areas for the various land covers. (**c-2**) shows the change in total area as a percentage of the initial value in both Ramsar sites and its surrounding areas for the various land covers where the percentage change is above 4%.

3.5. Case Study of Ramsar Site 549 (Zhalong) in Heilongjiang

A case study of the changes in urban areas and flooded vegetation at Ramsar site 549 (Zhalong) in Heilongjiang was used to further illustrate the effect of changes in the respective land cover types on the effective mesh size. There were no observable changes in urban area for the site and its surrounding area until 2001 (Figures S1 and S2). This was followed by an overall increase in its urban area in the years between 2001 and 2005 with a corresponding increase in the effective mesh size, which is indicative of decreased fragmentation. The best example of this change occurred between 2003 and 2004 when the increase in urban areas occurred adjacent to existing areas creating larger patches and an increased m_{eff} (Figures S1 and S2). In comparison, flooded vegetation covered significant areas both within the Ramsar site and its surrounding areas in 1992. Slight increases in the total area were first observed between 1998 and 2005 within the Ramsar site, with the majority of the increases occurring between 2006 and 2010 when large increases were observed. Many of these increases were located next to preexisting areas which led to their expansion. These changes in turn resulted in an increased m_{eff} indicating a decrease in fragmentation.

However, the majority of the changes in the surrounding areas occurred between 2004 and 2007. The changes in the surrounding area were also similar to those observed within the Ramsar site where increases in land cover were located next to preexisting areas

and resulted in a decrease in fragmentation as the m_{eff} increased (Figures S3 and S4). The changes in flooded vegetation between 2012 and 2013 were the only instances when an increase in fragmentation was observed as a result of a decrease in the land covered area. This change was a result of a decrease located in the southwest region of the surrounding area, which is highlighted in dark blue (Figure S3). The land cover loss connected several patches of flooded vegetation into a larger patch. With its removal, a decrease in the m_{eff} and an increase in fragmentation were observed.

3.6. Change Drivers Within Ramsar Sites and Its Surrounding Areas

Human footprint was the primary driver of land cover changes within the Chinese Ramsar sites for the majority of the period for which the change driver analysis was performed (2000 to 2019). As the dominant primary driver, the feature importance of human footprint fluctuated between 0.13 and 0.36 with an average of 0.24 out of a maximum of 1. This is in comparison to the annual average feature importance of 0.09, which remained similar throughout 2000 to 2019. Within the Ramsar sites, 2014 was the only year when the human footprint fell to 0.13 and became the secondary driver, while total precipitation (sum precipitation) became the primary driver as its relative importance increased to 0.16 (Figure 5).

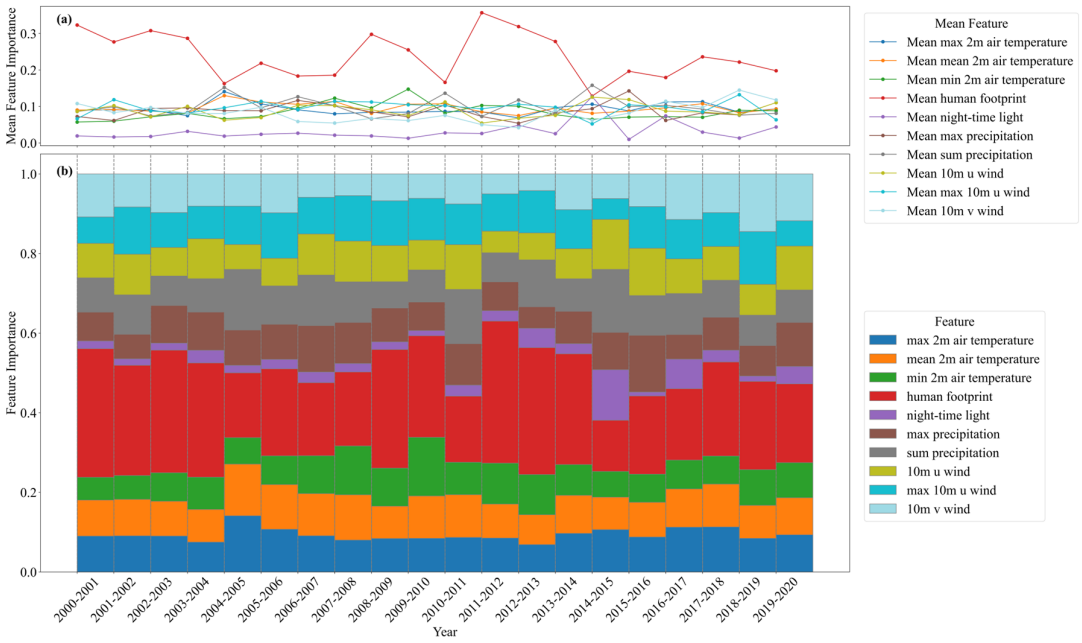

Figure 5. Temporal trends in feature importance in land cover lost or gained (Chinese Ramsar sites). Figure (**a**) shows the annual importance of various drivers over the 2000–2020 period. Figure (**b**) depicts stacked bar charts of the importance of drivers for each year from 2000 to 2020. The *X*-axis represents the year and the *Y*-axis represents the feature importance.

In comparison, human footprint was also the primary driver of changes in the surrounding areas throughout the entirety of the study period (Figure S5). While human footprint was the primary driver for both areas, the feature importance of human footprint in the surrounding areas had a smaller range between 0.16 and 0.32 and a slightly lower average of 0.23. Despite the minor differences, when comparing the two values year by year, the surrounding areas show a higher average than areas within the Ramsar site 65% of the time (Figure S5). This indicates a similar importance of human footprint as the primary driver for land cover change within the Ramsar sites and the surrounding areas, although it had a greater importance for the surrounding areas for the majority of the study period.

When only changes to wetlands were analyzed, human footprint remained the primary driver of changes within wetlands for both the Ramsar sites and the surrounding areas the majority of the time. However, there were fewer occurrences when it was the primary change driver. In contrast, there were 6 years (2004, 2006 to 2007, 2010 and 2018 to 2019) when human footprint was not the primary change driver for wetland changes when compared to the single year for all changes within Ramsar sites (Figures 5 and S6). During 2004, 2006, 2007 and 2010, total precipitation was the primary driver. In 2018, the E-W component of wind at 10 m (10 m u wind) was the primary driver and in 2019 maximum precipitation was the primary driver; 2014 was also unique as no changes were observed for wetlands.

In comparison, there were 8 years when the primary driver was not human footprint in the areas surrounding the Ramsar sites. These periods were observed in the surrounding areas in 2004, 2006, 2008, 2010, 2014 and 2016, 2017 and 2018 (Figure S7). Total precipitation was the primary driver in 2004, 2006 and 2014, while the maximum E-W component of wind at 10 m (10 m u wind) was the primary driver in 2008, 2010 and 2018. Night-time lights were also a primary driver in 2016 and 2017 (Figure S7). Similar to the results observed for all land cover changes, the surrounding areas had a higher feature importance than the areas within Ramsar sites for over 60% of the years within the study period.

3.7. Significance of Calculated Feature Importance

A series of two tailed T-tests comparing each of the possible drivers indicates that the calculated feature importance was statically significant (p-value < 0.005) for all pairings with human footprint. This was also true for the majority of pairings with night-time lights, with the exception of wetland changes in the surrounding area. For the changes observed both within Ramsar sites and in the surrounding areas, many of the calculated feature importances were statically significant (p-value < 0.05).

For most pairings between related drivers, such as the between min, mean and max air temperatures, the feature importance was often statistically insignificant (p-value $\geq$ 0.05). When all changes were considered, other pairings that were also insignificant for all air temperature drivers when paired with any components of wind, maximum precipitation, and sum precipitation. All components of wind when paired with maximum and sum precipitation were also statically insignificant.

When only considering wetland changes within Ramsar sites, the statistical test for the feature importance of pairings between air temperatures, precipitation drivers and components of wind show that all are generally insignificant. In contrast, pairings between either night-time lights or air temperature and all components of wind and precipitation for wetland changes in the surrounding areas it was found that their feature importance was statistically insignificant.

4. Discussions

A major challenge in this study was the inequitable distribution of Ramsar sites within the nine ecoregions and the eighteen administrative regions with provincial status in China. Since the selection of Ramsar sites was outside of this study's control, the resulting distribution bias was unavoidable. In order to address the bias within the area experiencing change in these regions, additional variables such as the percentage of specific land cover change within China, the percentage of total change within the ecoregion or provinces and the percentage of total change within China and were also computed. These provided additional insights into the distribution of the changes observed within different land covers, ecoregions and all Ramsar sites within China in order to address the distribution bias that is present.

Within the changes observed in land cover, grasslands and tree cover experienced some of the largest land cover changes within the Ramsar sites and their surrounding areas. The cumulative change in grasslands within the Ramsar sites was 2184.3 km^2 with an overall loss of 290.2 km^2, alongside a cumulative change of 1917.5 km^2 in the surrounding areas with an overall gain of 6.14 km^2. This highlights the challenges experienced by the environmental protection policies, which were started in 1998 and focused on the restoration of forest and grassland from marginal cropland [39–41]. Based on the current observations, these policies appear to have had a greater effect on the surrounding areas, although an overall loss was still observed in the two areas. Climatic simulations have also indicated that grasslands and shrublands have a greater vulnerability to climate change and carbon dioxide forcing [42,43]. These simulations raise serious concerns for the future of these land covers under the increasing stress of climate change. These predictions become even more dire as these land covers may also be a part of ecologically fragile wetland systems if they experience periodic flooding. In comparison, the overall loss of tree cover was the largest, at 547.3 km^2 within the Ramsar sites and 385.4 km^2 in the surrounding areas. These losses further illustrate the challenges China faces in its efforts to reverse the loss of tree cover through policies, afforestation and the increase in forest plantations and major forest projects concentrated in ecologically sensitive areas [39–41,44–47]. As with grasslands above, environmental protection policies that focus on the restoration of forest and grassland from marginal croplands also have little effect on tree cover as overall losses were observed for both areas as of 2020 [39–41].

Many of the largest changes were also observed within the most disturbed ecoregions and in some of the most vulnerable regions in China. In 1995, Hannah, Carr and Lankerani had already identified temperate grasslands and temperate broadleaf forest as two of the top five most disturbed eco-biomes [48]. Our observations are consistent with these earlier finding as the largest cumulative changes continue to be in the Mongolian–Manchurian Steppe and the Oriental Deciduous Forest ecoregions. These two ecoregions are part of the temperate grasslands and the temperate broadleaf forest biomed, respectively. Similarly, the largest overall changes were also observed within these two ecoregions with a few exceptions. These exceptions were located within the Manchu–Japanese Mixed Forest and the Tibetan Cold-winter deserts which are not only located within highly disturbed biomes, but are also in some of the most vulnerable regions in China's Northeast and on the Tibetan Plateau [36,49,50].

Heilongjiang and Tibet had some of the largest overall changed for many of the land covers examined. The changes observed with Heilongjiang were largely driven by the production of agricultural products such as timber and grains in addition to rising temperatures. As one of the provinces with the richest forest resources, where some of the last remaining large-scale forests are located, it was observed to have the second largest overall loss in land covers within its tree cover [51]. The province provides a third to half of China's timber needs and experienced mass deforestation in the mid 1990s and 2000s when China became a leading exporter of furniture and other finished wood products. In addition to state-sanctioned logging, 5000 km^2 of virgin forest are illegally logged per year in China [51]. Even with the implementation of logging bans for natural forests in 2015 and a 6.4% decrease in the logging quota by 2020, the overall changed observed continue to indicate a loss of tree cover within the Ramsar sites in Heilongjiang since 1992 [51]. In contrast to the losses observed in tree cover within Heilongjiang, the province also experienced large overall gains within croplands. Over the past three decades, climate warming shifts the 0 °C isoline, above which is a requirement for rice production, expanding the area suitable for its production [52]. The increase in croplands within Heilongjiang has been ongoing since the 1960s, with an average annual increase of 504 km^2, and slowed

to a rate of 379 km^2 per year between 1980 and 2000 [52]. By 2000, an additional site was encompassed by the 0 °C isoline. Since the adaptation of agricultural practice to warmer climatic conditions requires approximately 20 years, continued cropland expansion and increases in the overall gains within the province seem likely [52].

In comparison, both the largest overall land cover gain and the largest overall loss of land cover were observed in Tibet for water and grasslands, respectively. Due to the increasing temperature and precipitation brought about by climate change, a substantial increase in the terrestrial water storage was observed in the endorheic basins of Inner Tibet where both Ramsar sites in the province are located [53]. Within this region, the increase in terrestrial water storage was due to lake expansions that totaled 5.8 Gt per year from 2002 to 2017 [53]. Future predictions under mid-range emission scenarios suggest that Tibet is projected to experience even warmer climates by 2030, although terrestrial water storage in the lakes dominating Inner Tibet basin is projected to remain stable [53]. Tibet also has a long history of grassland degradations due to disturbances to the delicate equilibrium under which grasslands thrive. This remains a concern as the largest overall loss was observed in the Tibetan grasslands. These changes may be attributed to overgrazing and conversion to croplands in order to support the growing population [54]. Rapid climate change in the area has also exacerbated the problem, which has led to glacial retreats and lower groundwater tables [54]. These decrease the availability of water resulting in decreased biomass and further grassland degradations [54]. Once grassland degradation occurs, soil organic carbon and nutrients become more vulnerable to leaching and erosion, which in turn lead to changes in plant functional groups and a reduction in phosphorus which necessary for plant growth. These changes lead to further degradation where recovery is slow and uncertain [54]. Due to its slow recovery rate and the ever-increasing challenges, it is predicted that the Tibetan grasslands will disappear in the next 24–164 years [54].

5. Conclusions

Cumulatively, a total of 4000.2 km^2 of land within the Ramsar sites in China experienced land cover changes between 1992 and 2020. The largest overall changes observed were losses in tree cover (338.4 km^2) and grasslands (290.2 km^2), and an overall gain for flooded shrub or herbaceous cover (317.0 km^2). Of all the changes observed, many were concentrated in some of the most disturbed biomes and vulnerable regions within China [42,49,50]. The biomed with some of the largest changes include the Mongolian–Manchurian Steppe (temperate grasslands) and the Oriental Deciduous Forest (temperate broad-leaf forests). Provincially, land cover changes were also highly concentrated within Heilongjiang and Tibet. Due to the massive export of timber to meet ever-increasing demands, and the expansion of areas suitable for agriculture due to climate warming, Heilongjiang has experienced the greatest overall loss of tree cover along with the largest gains in croplands [51,52]. Comparatively, the increasing temperature and precipitation in Tibet have led to the largest gains in water, while the increasing population and rapid climate change have further exacerbated systemic grassland degradation leading to the largest overall loss in grasslands which are expected to disappear within the next 24–165 years [53,54].

The impact of human activities on protected areas and land cover change cannot be understated. The changes within the Ramsar sites were concentrated in areas closest to the sites' boundaries. The highest concentration of changes was predominantly located within the 5% buffer area closest to the site boundary with the greatest exposure human interaction. In provinces such as Anhui, Guangdong, Guangxi, Hong Kong, Liaoning, Shanghai and Zhejiang, over 70% of the changes occurred within the 5% buffer for certain land covers. These observations were especially noticeable for land covers inherently connected with human activity such as croplands and urban areas. In particular, all of the changes to urban

areas in Hong Kong and Shanghai were located within the 5% buffer. Notably, these two cities have Ramsar sites that are considered to have provincial status, allowing them to make the same types of decisions as other provinces.

The levels of fragmentation of flooded vegetation, water and urban areas were also greatly impacted by the existence of Ramsar sites. Initially, flooded vegetation and water had greater fragmentation within the Ramsar sites. In contrast, urban areas within the sites were more fragmented. Over the past three decades, fragmentation of flood vegetation has continued to decrease within Ramsar sites while it has increased in the surrounding areas. In comparison, the fragmentation of water increased both within Ramsar sites and its surrounding areas, although there is a greater level of fragmentation in the surrounding areas. Conversely, fragmentation in urban areas decreased overall, but its decrease in the areas surrounding Ramsar sites was three times greater than within. These changes further highlight the effectiveness of Ramsar sites as fragmentations within these sites were lower for flooded vegetation and water, and a higher fragmentation of urban areas was found compared to their surroundings.

Upon further analysis of the drivers causing these changes, human footprint was identified as the primary driver of land cover changes within Chinese Ramsar sites and their surrounding areas the majority of the time. A comparison of the change drivers for only wetland change indicated that while human footprints are still predominantly the primary driver, total precipitation was the second most frequent the primary driver within both areas. Despite the challenges faced by Ramsar sites, they continue to mitigate the effects of anthropogenic changes and continue to be more stable than their surrounding areas, with an overall improvement in wetland areas with lower levels of fragmentation over the past three decades.

Supplementary Materials: The following supporting information can be downloaded at: https://www.mdpi.com/article/10.3390/rs17050896/s1.

Author Contributions: Conceptualization, K.K.Y.C., Y.B. and B.X.; methodology, K.K.Y.C., Z.R., Y.L. and H.S.; writing—original draft preparation, K.K.Y.C.; writing—review and editing, K.K.Y.C., Z.R., Y.L., H.S., Y.B. and B.X. All authors have read and agreed to the published version of the manuscript.

Funding: This research was funded by the Project of Shanghai Municipal Commission of Science and Technology, grant number 22dz1209602 and the National Key Research and Development Program of China, grant number 2022YFE0209300, and 2022YFB3903703.

Data Availability Statement: The data presented in this study have been included in the Supplemental Data provided. These data were derived from the following resources available in the public domain as cited within the article.

Conflicts of Interest: The authors declare no conflicts of interest. The funders had no role in the design of the study; in the collection, analyses, or interpretation of data; in the writing of the manuscript; or in the decision to publish the results.

References

1. Davidson, N.C. How much wetland has the world lost? Long-term and recent trends in global wetland area. *Mar. Freshw. Res.* **2014**, *65*, 934–941. [CrossRef]
2. Bino, G.; Kingsford, R.T.; Brandis, K. Australia's wetlands–learning from the past to manage for the future. *Pac. Conserv. Biol.* **2016**, *22*, 116–129. [CrossRef]
3. Mitra, S.; Wassmann, R.; Vlek, P.L. Global inventory of wetlands and their role in the carbon cycle. In *ZEF–Discussion Papers on Development Policy No. 64, Center for Development Research*; Zentrum für Entwicklungsforschung (ZEF): Bonn, Germany, 2003. [CrossRef]
4. Bridgewater, P. A New Context for the Ramsar Convention: Wetlands in a Changing World. *Rev. Eur. Community Int. Environ. Law* **2008**, *17*, 100–106. [CrossRef]

5. Matthews, G.V.T. *The Ramsar Convention on Wetlands: Its History and Development*; Ramsar Convention Bureau: Gland, Switzerland, 1993.
6. Brooks, R.P.; Serfass, T.L.; Triska, M.; Rebelo, L.M. Ramsar Protected Wetlands of International Importance as Habitats for Otters. In Proceedings of XIth International Otter Colloquium, IUCN Otter Specialist Group Bulletin B, Pavia, Italy, 30 August–4 September 2011; Volume 28, pp. 47–63.
7. Wu, T.; Perrings, C.; Shang, C.; Collins, J.P.; Daszak, P.; Kinzig, A.; Minteer, B.A. Protection of wetlands as a strategy for reducing the spread of avian influenza from migratory waterfowl. *Ambio* **2019**, *49*, 939. [CrossRef]
8. Everard, M.; Kangabam, R.; Tiwari, M.K.; McInnes, R.; Kumar, R.; Talukdar, G.H.; Dixon, H.; Joshi, P.; Allan, R.; Joshi, D.; et al. Ecosystem service assessment of selected wetlands of Kolkata and the Indian Gangetic Delta: Multi-beneficial systems under differentiated management stress. *Wetl. Ecol. Manag.* **2019**, *27*, 405–426. [CrossRef]
9. Finlayson, C.M.; Davidson, N.C.; Spiers, A.G.; Stevenson, N.J. Global wetland inventory; current status and future priorities. *Mar. Freshw. Res.* **1999**, *50*, 717–727. [CrossRef]
10. Seto, K.C.; Fragkias, M. Mangrove conversion and aquaculture development in Vietnam: A remote sensing-based approach for evaluating the Ramsar Convention on Wetlands. *Glob. Environ. Change* **2007**, *17*, 486–500. [CrossRef]
11. Kermode, S.J.; Heijnis, H.; Wong, H.; Zawadzki, A.; Gadd, P.; Permana, A. A Ramsar-wetland in suburbia: Wetland management in an urbanised, industrialised area. *Mar. Freshw. Res.* **2016**, *67*, 771–781. [CrossRef]
12. Diamond, J.M.; Bishop, K.D.; Van Balen, S. Bird Survival in an Isolated Javan Woodland: Island or Mirror? *Conserv. Biol.* **1987**, *1*, 132–142. [CrossRef]
13. Jones, D.A.; Hansen, A.J.; Bly, K.; Doherty, K.; Verschuyl, J.P.; Paugh, J.I.; Carle, R.; Story, S.J. Monitoring land use and cover around parks: A conceptual approach. *Remote Sens. Environ.* **2009**, *113*, 1346–1356. [CrossRef]
14. Schonewald-Cox, C.M. Boundaries in the Protection of Nature Reserves: Translating Multidisciplinary Knowledge into Practical Conservation. *BioScience* **1988**, *38*, 480–486. [CrossRef]
15. Hansen, A.J.; DeFries, R. Ecological mechanisms linking protected areas to surrounding lands. *Ecol. Appl.* **2007**, *17*, 974–988. [CrossRef] [PubMed]
16. Janzen, D.H. No park is an island: Increase in interference from outside as park size decreases. *Oikos* **1983**, *41*, 402–410. [CrossRef]
17. Laurance, W.F. Edge effects in tropical forest fragments: Application of a model for the design of nature reserves. *Biol. Conserv.* **1991**, *57*, 205–219. [CrossRef]
18. Hu, S.; Niu, Z.; Chen, Y.; Li, L.; Zhang, H. Global wetlands: Potential distribution, wetland loss, and status. *Sci. Total Environ.* **2017**, *586*, 319–327. [CrossRef]
19. The World Bank Group. Land Area (sq. km)-China [Data Set]. World Bank Open Data. 2021. Available online: https://data.worldbank.org/indicator/AG.LND.TOTL.K2?locations=CN (accessed on 21 January 2021).
20. Niu, Z. Mapping China's Wetlands and Recent Changes with Remotely Sensed Data. In *Remote Sensing of Wetlands: Applications and Advances*; Tiner, R.W., Lang, M.W., Klemas, V.V., Eds.; CRC Press: Boca Raton, FL, USA, 2015; pp. 473–490.
21. An, S.; Li, H.; Guan, B.; Zhou, C.; Wang, Z.; Deng, Z.; Zhi, Y.; Liu, Y.; Xu, C.; Fang, S.; et al. China's Natural Wetlands: Past Problems, Current Status, and Future Challenges. *AMBIO A J. Hum. Environ.* **2007**, *36*, 335–342. [CrossRef]
22. Protected Planet. Explore Protected Areas and OECMs [Data Set]. Protected Planet. 2020. Available online: https://www.protectedplanet.net/en/search-areas?geo_type=site (accessed on 29 September 2019).
23. Ramsar Convention Secretariat. Ramsar Sites Information Service [Data Set]. Ramsar Sites Information Service. 2019. Available online: https://rsis.ramsar.org (accessed on 29 September 2019).
24. Dugge, J. Buffer by Percentage (Version 0.3.3). 2020. Available online: https://plugins.qgis.org/plugins/BufferByPercentage (accessed on 13 October 2020).
25. Davis, J.; Brock, M. Detecting unacceptable change in the ecological character of Ramsar wetlands. *Ecol. Manag. Restor.* **2008**, *9*, 26–32. [CrossRef]
26. Fournier, R.A.; Grenier, M.; Lavoie, A.; Hélie, R. Towards a strategy to implement the Canadian Wetland Inventory using satellite remote sensing. *Can. J. Remote Sens.* **2007**, *33* (Suppl. 1), S1–S16. [CrossRef]
27. SDRN F U. Udvardy's Ecoregions [Data Set]. Food and Agriculture Organization of the United Nations. 2002. Available online: http://www.fao.org/geonetwork/srv/en/metadata.show?id=1008&currTab=simple (accessed on 9 October 2019).
28. Spalding, M.D.; Fox, H.E.; Allen, G.R.; Davidson, N.; Ferdaña, Z.A.; Finlayson, M.; Halpern, B.S.; Jorge, M.A.; Lombana, A.; Lourie, S.A.; et al. Marine Ecoregions of the World: A Bioregionalization of Coastal and Shelf Areas. *BioScience* **2007**, *57*, 573–583. [CrossRef]
29. Defourny, P.; Lamarche, C.; Brockmann, C.; Boettcher, M.; Bontemps, S.; De Maet, T.; Duveiller, G.L.; Harper, K.; Hartley, A.; Kirches, G.; et al. Observed annual global land-use change from 1992 to 2020 three times more dynamic than reported by inventory-based statistics. 2023; *in preparation*. Available online: https://maps.elie.ucl.ac.be/CCI/viewer/download.php (accessed on 6 September 2019).

30. ESA. Land Cover CCI Product User Guide Version 2. Tech. Rep. 2017. Available online: https://maps.elie.ucl.ac.be/CCI/viewer/download/ESACCI-LC-Ph2-PUGv2_2.0.pdf (accessed on 6 September 2019).
31. Yang, J.; Huang, X. 30 m annual land cover and its dynamics in China from 1990 to 2019. *Earth Syst. Sci. Data* **2021**, *2021*, 3907–3925. [CrossRef]
32. Zhang, X.; Zhao, T.; Xu, H.; Liu, W.; Wang, J.; Chen, X.; Liu, L. GLC_FCS30D: The first global 30 m land-cover dynamics monitoring product with a fine classification system for the period from 1985 to 2022 generated using dense-time-series Landsat imagery and the continuous change-detection method. *Earth Syst. Sci. Data* **2024**, *16*, 1353–1381. [CrossRef]
33. Jaeger, J.A. Landscape division, splitting index, and effective mesh size: New measures of landscape fragmentation. *Landsc. Ecol.* **2000**, *15*, 115–130. [CrossRef]
34. Bosch, M. PyLandStats: An open-source Pythonic library to compute landscape metrics. *PLoS ONE* **2019**, *14*, e0225734. [CrossRef] [PubMed]
35. Hersbach, H.; Bell, B.; Berrisford, P.; Hirahara, S.; Horányi, A.; Muñoz-Sabater, J.; Nicolas, J.; Peubey, C.; Radu, R.; Schepers, D.; et al. The ERA5 global reanalysis. *Q. J. R. Meteorol. Soc.* **2020**, *146*, 1999–2049. [CrossRef]
36. Li, X.; Zhou, Y.; Zhao, M.; Zhao, X. A harmonized global nighttime light dataset 1992–2018. *Sci. Data* **2020**, *7*, 168. [CrossRef]
37. Mu, H.; Li, X.; Wen, Y.; Huang, J.; Du, P.; Su, W.; Miao, S.; Geng, M. A global record of annual terrestrial Human Footprint dataset from 2000 to 2018. *Sci. Data* **2022**, *9*, 176. [CrossRef]
38. Menze, B.H.; Kelm, B.M.; Masuch, R.; Himmelreich, U.; Bachert, P.; Petrich, W.; Hamprecht, F.A. A comparison of random forest and its Gini importance with standard chemometric methods for the feature selection and classification of spectral data. *BMC Bioinform.* **2009**, *10*, 213. [CrossRef]
39. Liu, M.; Tian, H. China's land cover and land use change from 1700 to 2005: Estimations from high-resolution satellite data and historical archives. *Glob. Biogeochem. Cycles* **2010**, *24*, GB3003. [CrossRef]
40. Zhang, P.; Shao, G.; Zhao, G.; Le Master, D.C.; Parker, G.R.; Dunning, J.B., Jr.; Li, Q. China's forest policy for the 21st century. *Science* **2000**, *288*, 2135–2136. [CrossRef]
41. Zhang, Y.; Song, C. Impacts of afforestation, deforestation, and reforestation on forest cover in China from 1949 to 2003. *J. For.* **2006**, *104*, 383–387. [CrossRef]
42. Ni, J. Impacts of climate change on Chinese ecosystems: Key vulnerable regions and potential thresholds. *Reg. Environ. Change* **2011**, *11*, 49–64. [CrossRef]
43. Chen, M.; Pollard, D.; Barron, E.J. Regional climate change in East Asia simulated by an interactive atmosphere–soil–vegetation model. *J. Clim.* **2004**, *17*, 557–572. [CrossRef]
44. Ahrends, A.; Hollingsworth, P.M.; Beckschäfer, P.; Chen, H.; Zomer, R.J.; Zhang, L.; Wang, M.; Xu, J. China's fight to halt tree cover loss. *Proc. R. Soc. B Biol. Sci.* **2017**, *284*, 20162559. [CrossRef] [PubMed]
45. Houghton, R.A.; Hackler, J.L. Sources and sinks of carbon from land-use change in China. *Glob. Biogeochem. Cycles* **2003**, *17*, 1034. [CrossRef]
46. State Forestry Administration China. China National Progress Report to the UNFF Secretariat on the Implementation of NLBI and Other Relevant Resolutions. 2011. Available online: http://www.unece.lsu.edu/certificate_eccos/documents/2013Mar/ce13_07.pdf (accessed on 11 January 2022).
47. Wang, G.; Innes, J.L.; Lei, J.; Dai, S.; Wu, S.W. China's forestry reforms. *Science* **2007**, *318*, 1556–1557. [CrossRef]
48. Hannah, L.; Carr, J.L.; Lankerani, A. Human disturbance and natural habitat: A biome level analysis of a global data set. *Biodivers. Conserv.* **1995**, *4*, 128–155. [CrossRef]
49. Weng, E.S.; Zhou, G.S. Modeling distribution changes of vegetation in China under future climate change. *Environ. Model. Assess.* **2006**, *11*, 45–58. [CrossRef]
50. Yu, L.; Cao, M.; Li, K. Climate-induced changes in the vegetation pattern of China in the 21st century. *Ecol. Res.* **2006**, *21*, 912–919. [CrossRef]
51. Yemo, Z. Environmental policy in china: Forest management and development in heilongjiang province. *Contemp. Chin. Political Econ. Strateg. Relat.* **2021**, *7*, 1775–1808, XXII–XXIII.
52. Gao, J.; Liu, Y. Climate warming and land use change in Heilongjiang Province, Northeast China. *Appl. Geogr.* **2011**, *31*, 476–482. [CrossRef]
53. Li, X.; Long, D.; Scanlon, B.R.; Mann, M.E.; Li, X.; Tian, F.; Sun, Z.; Wang, G. Climate change threatens terrestrial water storage over the Tibetan Plateau. *Nat. Clim. Change* **2022**, *12*, 801–807. [CrossRef]
54. Liu, S.; Zamanian, K.; Schleuss, P.M.; Zarebanadkouki, M.; Kuzyakov, Y. Degradation of Tibetan grasslands: Consequences for carbon and nutrient cycles. *Agric. Ecosyst. Environ.* **2018**, *252*, 93–104. [CrossRef]

Disclaimer/Publisher's Note: The statements, opinions and data contained in all publications are solely those of the individual author(s) and contributor(s) and not of MDPI and/or the editor(s). MDPI and/or the editor(s) disclaim responsibility for any injury to people or property resulting from any ideas, methods, instructions or products referred to in the content.